SCIENTIFIC REPORTS

OPEN

SUBJECT AREAS:
ELECTRICAL AND ELECTRONIC ENGINEERING
NANOSCALE MATERIALS

Received
8 April 2014

Accepted
2 June 2014

Published
20 June 2014

Correspondence and requests for materials should be addressed to J.M. (jens.meyer@philips.com)

Metal Oxide Induced Charge Transfer Doping and Band Alignment of Graphene Electrodes for Efficient Organic Light Emitting Diodes

Jens Meyer[1], Piran R. Kidambi[2], Bernhard C. Bayer[2], Christ Weijtens[1], Anton Kuhn[1], Alba Centeno[3], Amaia Pesquera[3], Amaia Zurutuza[3], John Robertson[2] & Stephan Hofmann[2]

[1]Philips Research, Philipsstrasse 8, 52068 Aachen, Germany, [2]Department of Engineering, University of Cambridge, 9 JJ Thomson Avenue, Cambridge CB3 0FA, UK, [3]Graphenea S.A, Tolosa Hiribidea 76, E-20018 Donostia San Sebastian, Spain.

The interface structure of graphene with thermally evaporated metal oxide layers, in particular molybdenum trioxide (MoO_3), is studied combining photoemission spectroscopy, sheet resistance measurements and organic light emitting diode (OLED) characterization. Thin (<5 nm) MoO_3 layers give rise to an 1.9 eV large interface dipole and a downwards bending of the MoO_3 conduction band towards the Fermi level of graphene, leading to a near ideal alignment of the transport levels. The surface charge transfer manifests itself also as strong and stable p-type doping of the graphene layers, with the Fermi level downshifted by 0.25 eV and sheet resistance values consistently below 50 Ω/sq for few-layer graphene films. The combination of stable doping and highly efficient charge extraction/injection allows the demonstration of simplified graphene-based OLED device stacks with efficiencies exceeding those of standard ITO reference devices.

Materials combining high electrical conductivity and optical transparency are vital for opto-electronic devices, such as solar cells, light emitting diodes and touch screens[1,2]. Doped metal oxides, in particular indium tin oxide (ITO), are thereby currently the most widely used. However, the rising price of Indium and the desire for flexible substrates necessitates alternative transparent conductor materials (TCs) for next generation devices. Among the range of intensely studied emerging TCs, graphene grown by scalable chemical vapor deposition (CVD) shows great promise as its two-dimensional bonding configuration offers flexibility, mechanical robustness and chemical inertness combined with unusual electrical and optical properties[1,3,4]. All these properties are thereby support and interface dependent, as graphene is atomically thin[5]. As widely highlighted in the literature[6], graphene supports a relatively high electronic mobility, but it is intrinsically not a highly conductive electrode material due to the low charge carrier concentration. Hence stable doping of graphene layers is crucial to achieve sheet resistance values below 100 Ω/sq with optical transmissivity above 90%[4,7]. This links to substantial shifts in the work function of graphene.

There are numerous recent reports highlighting promising results with graphene based electrodes, in particular for organic electronic applications such as organic photovoltaic cells and organic light emitting diodes (OLEDs)[8–15]. For these applications band engineering and efficient charge extraction and injection across the electrode/organic interfaces are at least as important as the sheet resistance of the TC. To reduce interfacial barriers, hole injection layers (HIL) are widely used, in particular based on transition metal oxide films such as molybdenum trioxide (MoO_3), which unlike poly (3,4-ethylenedioxythiophene): poly (styrenesulfonate) (PEDOT:PSS) do not cause device degradation[16]. While such interfacial transition metal oxide films are becoming widely used for graphene electrodes, the focus of the discussion thereby has been either on stable doping or improved wetting[11–12,17–19] and there are currently few reports that address a fundamental understanding of the interfacial electronic structure[20].

Here, we report a detailed study of the interface structure of graphene with thermally evaporated MoO_3 layers, with the motivation of understanding the full functionality of these interfaces and the related electronic structure, which is of key importance to organic electronics. We focus on CVD graphene layers transferred to display glass or oxide support, and systematically combine photoemission spectroscopy, sheet resistance measurements and

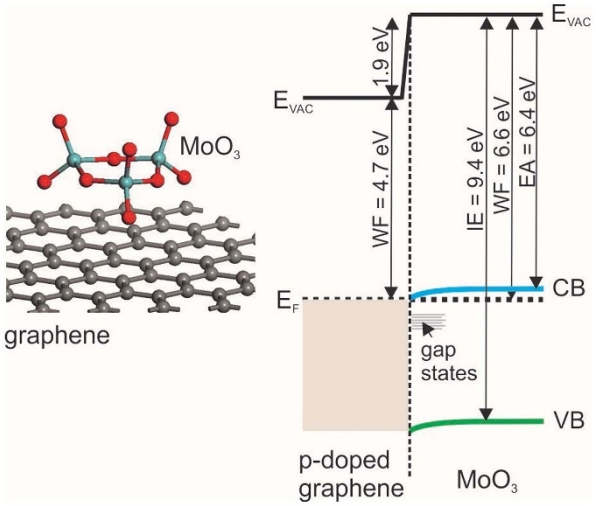

Figure 1 | Schematic of graphene/MoO_3 interface and energy level alignment diagram of the monolayer graphene/MoO_3 interface. The CB position was calculated using the band gap determined from our UPS data and inverse photoemission spectroscopy measurements as given in Ref 16.

the characterization of OLED device stacks. Incorporating the recently improved understanding of the electronic structure of MoO_3[16], our data shows that thin (<5 nm) MoO_3 layers give rise to a very large 1.9 eV interface dipole and a downwards bending of the MoO_3 conduction band towards the Fermi level of graphene, which lead to a near ideal alignment of the transport levels. Thus, the charge injection barrier is almost zero and the energy level alignment is reminiscent of that of a classical ohmic metal/n-type semiconductor junction. The surface charge transfer manifests itself also as strong p-type doping of the graphene layers, with a C1s core level shift of 0.25 eV reflecting the downshift of the Fermi level with respect to the graphene Dirac point. This charge transfer doping is reasonably stable with environment and temperature, and our sheet resistance measurements consistently show values of below 50 Ω/sq for few-layer graphene (FLG) films. The combination of stable doping and highly efficient charge extraction and injection allows us to demonstrate simplified graphene-based OLED device stacks without additional PEDOT interlayers with efficiencies exceeding those of standard ITO reference devices.

Results and Discussion

Fig. 1 shows a schematic of the MoO_3/graphene interface and its electronic structure. It is important to note that due to oxygen vacancies MoO_3 is a highly n-doped semiconductor exhibiting very deep lying electronic states, which has only recently been shown and has led to a reinterpretation of the role of such transition metal oxide films in organic electronic devices[21]. The electron affinity and work function (WF) of MoO_3 are > 6 eV, as highlighted in Figure 1. It should also be emphasized that it is in fact the band level alignment that is crucial to the device functionality and not whether the TC is p-type or n-type. Using combined ultraviolet and x-ray photoemission spectroscopy (UPS, XPS) allows us to unambiguously determine the key features of the interface energetics.

Fig. 2 shows UPS spectra of monolayer graphene on a Si/SiO_2 (300 nm) wafer with incrementally deposited MoO_3 layers on top. The graphene was grown by catalytic low-pressure CVD on commercial Cu foil and was subsequently transferred to the Si/SiO_2 support (see Experimental Section)[5,22]. As-synthesized graphene is inherently poly-crystalline with a domain size distribution centered around ~10 μm[22,23]. The transferred graphene films are optically homogeneous with an average Raman I_D/I_G ratio of ~0.05–0.06 and I_{2D}/I_G ratio of > 1 (see Supp. Information S1), indicative of a high crystalline quality as reported previously[22]. The MoO_3 layers were thermally evaporated in high vacuum (base pressure ≈10^{-6} mbar) at a rate of 0.1–0.3 Å/sec. Figure 2b displays the full measured spectrum, whereas Figures 2a and 2c show magnified sections of the secondary electron cutoff and the valence band states, respectively. From the secondary electron cutoff at high binding energy the work function (WF) can be calculated, and the edge of the valence band determines the VB onset; the resulting positions are marked with ticks in Fig. 2. The secondary electron cutoff of as-transferred monolayer graphene is at −16.8 eV, corresponding to a work function of 4.4 eV, in good agreement to previous literature[13]. A closer look at the valence band states of the as-transferred SiO_2 supported monolayer graphene reveals that they extend towards the Fermi level (shown as dotted line with 20-fold magnification in Figure. 2c), as expected from a zero-band gap material.

The deposition of MoO_3 on graphene shifts the secondary electron cutoff towards lower kinetic energy which is equivalent to an increasing WF. A rapid shift can be observed during the deposition of the first few Angstroms while saturation occurs between 22–46 Å (Figure 2a). In addition, our XPS analysis (Fig. 3) indicates a decrease in the binding energy (BE) of the respective C1s core level spectra of

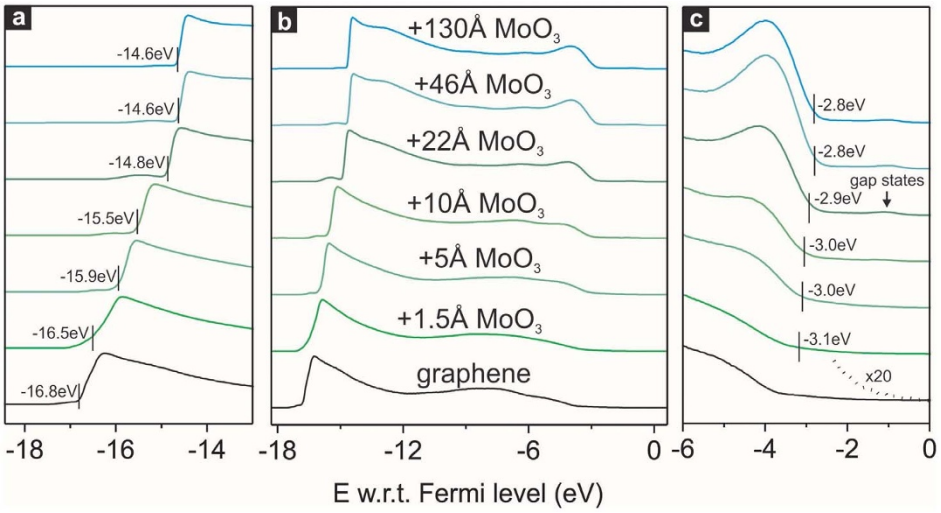

Figure 2 | UPS spectra plotted with respect to Fermi level of monolayer graphene with incrementally deposited MoO_3 layers. (a) Magnified view of photoemission onset. (b) Full spectrum. (c) Magnified view of the valence band states (dotted line shows UPS spectrum of graphene near the Fermi level with additional 20-fold magnification). Ticks mark the position of the cut-off and valence band edges.

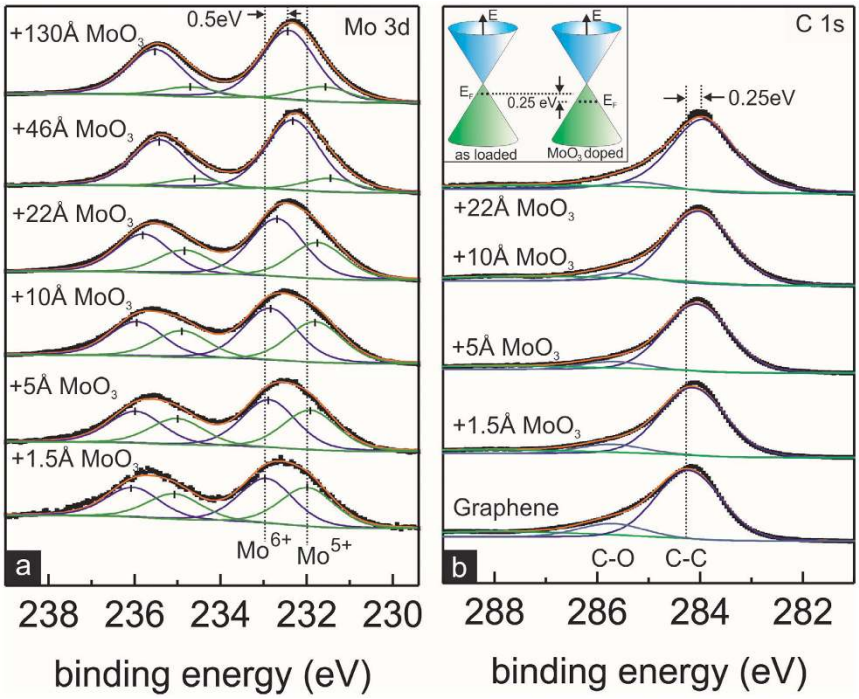

Figure 3 | XPS spectra of monolayer graphene with incrementally increased MoO_3 layer thickness. (a) Mo 3d core level spectra with marked positions of the Mo^{5+} and Mo^{6+} states. (b) C 1s core levels with marked positions of the C-C bond and the shift of this position upon MoO_3 deposition. The additional broad peak can be attributed to carbon-oxygen bonding as an effect of defect states and air-exposure. Inset: Schematic of graphene Fermi-Dirac cone illustrating the Fermi level shift due to the charge transfer process from MoO_3. The as-grown and transferred monolayer graphene on the SiO_2 substrate prior to MoO_3 deposition is slightly p-doped due to air-exposure.

graphene, corresponding to a WF increase of ~0.25 eV due to the MoO_3 coverage. The shift of the UPS secondary electron cutoff corresponds to the formation of a large interface dipole, caused by an electron transfer from graphene to MoO_3. This charge transfer process induces p-doping of graphene as a result of Fermi level alignment across the interface, as illustrated in Fig. 1. Fig. 2 shows that with increasing MoO_3 layer thickness the valence band edge of the metal oxide moves 0.3 eV closer to the Fermi level which can be attributed to band bending. Analogous to the secondary electron cutoff, the shift of the valence band saturates after deposition of a few monolayers (22–46Å). At this point, the valence band edge is 2.8 eV below the Fermi level, thus the ionization energy of MoO_3, defined as the energy difference between the vacuum level and the valence band edge, is 9.4 eV, consistent with reports in literature[21]. With increasing MoO_3 layer thickness an additional broad gap state with its maximum around 1 eV below the Fermi level can be observed, as marked in Figure 2c. In previous reports this has been attributed to a reduced oxidation state[24,25]. We will discuss the origin in more detail along with the XPS analysis (Fig. 3).

Having studied the doping effect in graphene we now proceed to determine the injection barrier between graphene and MoO_3 for which the energetic difference between the transport levels of both materials has to be determined. The charge transport level in graphene is given by its Fermi level position and MoO_3 is a n-doped semiconductor and hence electron transport takes place in the conduction band (CB)[21]. The large upwards shift of the vacuum level as a result of the interface dipole and the downwards bending of the MoO_3 conduction band towards the Fermi level of graphene lead to a near ideal alignment of the transport levels. Thus, the charge injection barrier is almost zero, as this is schematically depicted in Fig. 1. We note that the energy level alignment here is reminiscent of that of a classical ohmic metal/n-type semiconductor junction. On the other hand, it has been often reported that MoO_3 causes strong band bending into the bulk of organic semiconductors, like CBP, and C_{60}[16,26]. For monolayer graphene, the hole-doping is strongly localized in the monolayer and the charge compensation is established by an electron exchange into the bulk of MoO_3. This has been verified by synchrotron photoemission spectroscopy for epitaxial graphene on SiC[17].

Fig. 3 focuses on the XPS core level signatures at the graphene/MoO_3 interface, with the evolution of Mo 3d and C 1s core levels plotted for incrementally increased MoO_3 thickness. A thick layer (13 nm) of MoO_3 film features two main peaks at 232.4 eV and 235.5 eV, related to the Mo $3d_{3/2}$ and $3d_{5/2}$ components (Fig. 3a) and indicative of a predominant Mo^{6+} oxidation state. Two additional small peaks arise at ~234.7 eV and ~231.6 eV, respectively, which can be assigned to a reduced MoO_x (Mo^{5+}) species. At the very interface the amount of Mo^{5+} species increases significantly as a result of a strong reduction process induced by the graphene. We propose that these reduced MoO_x species cause the increased gap state density in the UPS spectra (Fig. 2). Kanai et al. showed that the Mo^{5+} oxidation states occurred when organic molecules were adsorbed on the metal oxide surface[24]. This has also been verified by density functional theory study of a MoO_x/4,4′-*N*,*N*′-dicarbazolebiphenyl (CBP) interface[27]. In addition, it has been demonstrated that air-exposure of MoO_3 also leads to a reduction process which not only changes the stoichiometry at the surface, but also lowers the WF significantly[28,29].

We observe similar shifts of ~0.5 eV in the Mo^{6+} and Mo^{5+} states towards lower binding energies with increasing MoO_3 thickness, consistent with an electron transfer from the graphene to the metal oxide, i.e. a p-type charge transfer doping of graphene. Interestingly, this shift is larger than the valence band bending as measured by UPS. Considering the information depth of XPS is larger than that of UPS (based on the excitation energies used here), the data indicates that the band bending might be even stronger at the very interface. However, the UPS analysis identified already pinning of the CB at the Fermi level. An even stronger downward shift of the CB would imply

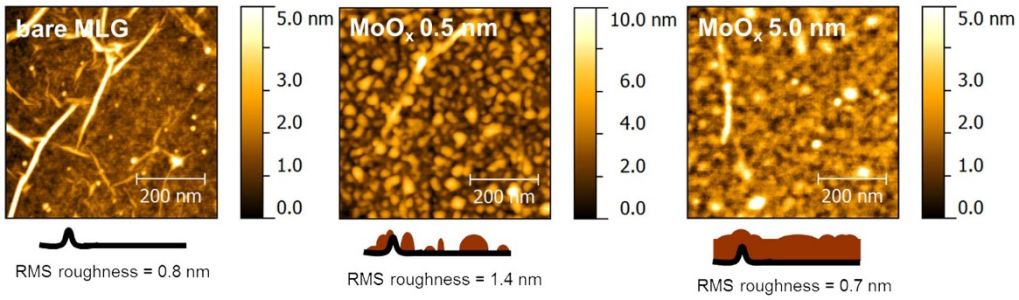

Figure 4 | AFM images measured in non-contact mode of (a) as transferred monolayer graphene, (b) + 0.5 nm MoO_3 and (c) + 5 nm MoO_3. Schematic sketches are not to scale.

a scenario in which the CB is placed below the Fermi level. Thus, a degenerate metal oxide interface is formed; an effect which is well-known in classical inorganic metal/n-type semiconductors. Note, that recently Hu et al.[20] investigated the graphene/MoO_3 interface of graphene supported on a Cu catalyst foil using photoemission spectroscopy. However, they did not observe a shift of the Mo 3d peaks, which might be attributed to interactions with the Cu surface[5,20]. Further, we have recently shown that graphene on Cu can be n-doped by up to 0.35 eV (XPS C1s core level shift from 284.4 to 284.75 eV) depending on the levels of oxygen intercalation[5]. This reflects the critical importance of support effects for graphene electrodes. Hence, we focus here on CVD graphene layers transferred to device relevant substrates to study the clear implication of these effects at realistic device working conditions.

Fig. 1 highlights the measured interface energetics: MoO_3 molecules on a graphene surface induce a surface charge transfer that nearly perfectly aligns the transport level for an efficient charge injection into devices. Fig. 3b shows that the C 1s core level signatures shift around 0.25 eV towards lower binding energy with increasing MoO_3 layer thickness. This is another clear indication of strong p-type transfer doping of graphene. The corresponding band structure (Dirac cone) before and after MoO_3 doping is illustrated in the inset of Fig. 3b. The exact position of the Fermi level cannot be detected due to the limited resolution of the UPS/XPS system. However, the C1s core level shift of 0.25 eV after MoO_3 doping implies that the Fermi level shifts lower with respect to the graphene Dirac point, which corresponds to an increase of the graphene WF from 4.4 eV to 4.7 eV (Fig. 3b). This shift is significantly larger compared to reported values of ≈0.12 eV for HNO_3 doping of graphene[30]. We note that a high density of states near the Fermi level is of particular importance for efficient hole-injection, since OLEDs require high current densities at low voltages.

Fig. 4 displays atomic force microscope (AFM) images of the metal oxide layer formation process on graphene. The surface of as-transferred and SiO_2 supported graphene shows wrinkles along with PMMA residuals and gives an average RMS roughness value of ≈0.8 nm (Fig. 4a). After evaporation of ≈0.5 nm of MoO_3 (Fig. 4b), the AFM images show MoO_3 nanoparticles decorating the MLG surface, indicative of a Volmer-Weber type nucleation mode. A thickness of around 2 nm corresponds to the onset of the formation of a continuous MoO_3 film, consistent with the saturation of the doping effect as seen from our XPS and UPS measurements. The graphene surface covered with approx. 5 nm of MoO_3 results in an RMS roughness value of ≈0.7 nm, as depicted in Fig. 4c.

Our photoemission spectroscopy results reveal that thin, thermally evaporated MoO_3 layers allow an efficient charge transfer doping of graphene. This is verified by in-situ sheet resistance measurements of graphene upon MoO_3 deposition, as shown in Fig. 5. The measurements were carried out with 4-point probe measurements without breaking the vacuum. The initial sheet resistance of as supported monolayer graphene was measured to be ~700 Ω/sq on average (values varied between 400 Ω/sq and 1 kΩ/sq). We emphasize that the sheet resistance values here refer to a 4-point probe geometry with 1 mm distance between the probes, including many graphene domain boundaries and wrinkles, hence a large error bar is expected. Further, this initial sheet resistance value is strongly influenced by unintentional doping due to air exposure and exposure to process chemicals (intrinsic graphene mono-layer has sheet resistance of the order of 6 kΩ/sq)[31]. This is a general challenge reported for graphene films across the literature and is corroborated here by the fact that the graphene sheet resistance increases upon transfer into vacuum and subsequent vacuum annealing, resulting in an increased sheet resistance of ~1.1 kΩ/sq after vacuum annealing at 140°C. Fig. 5 shows that the deposition of a few Angstrom of MoO_3 drastically lowers the graphene sheet resistance whereby saturation occurs for approx. 3–4 nm MoO_3 consistent with our UPS/XPS and AFM data. The sheet resistance of MoO_3 doped graphene remains unchanged upon further annealing in vacuum. Stable doping is important for OLED applications, where reliable operation is required at elevated temperatures like for instance in the automotive sector. The doping is also stable in air. We only observe a ~10% increase in sheet resistance after storage in air for several hours. Such high stability has also been reported for MoO_x-doped carbon nanotubes with sheet resistance changes less than 10% over 20 days in ambient[19]. Xie et al., on the other hand, observed a strong change of the MoO_3 doping efficiency which might be attributed to a different stoichiometry[18].

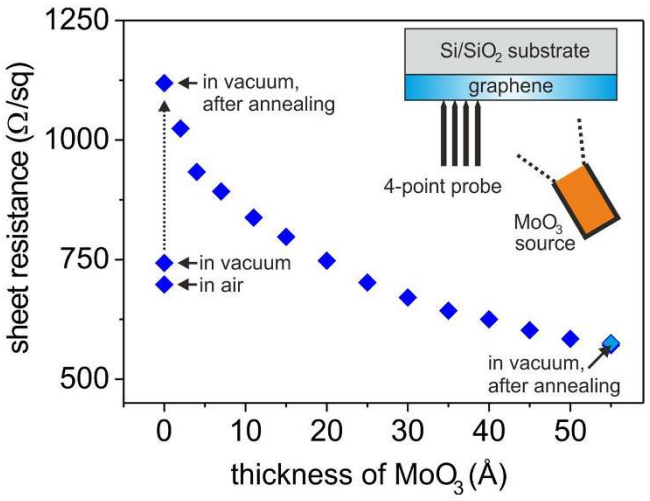

Figure 5 | In-situ sheet resistance measurements of monolayer graphene. Measurement sequence: in air, in vacuum, after annealing at 140°C in vacuum, upon deposition of MoO_3, after annealing at 140°C. The surface charge transfer doping leads to a rapid lowering of the sheet resistance upon deposition of a few Å of MoO_3. The MoO_3 doped graphene remains nearly unchanged when annealed at 140°C (overlap of dark and light blue diamond). Inset shows in-situ 4-point probe setup.

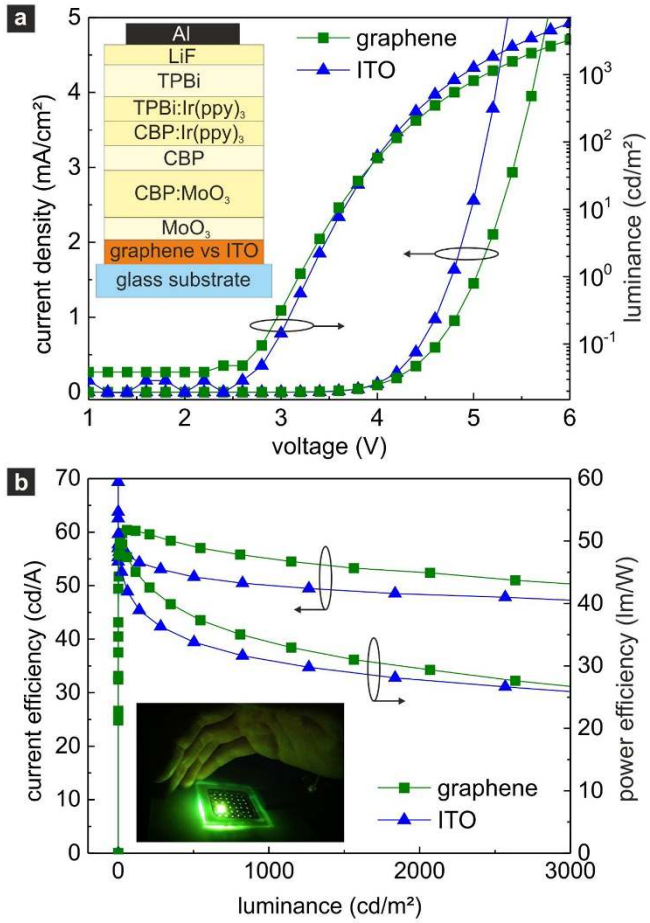

Figure 6 | Device characteristics of OLED stacks with either monolayer graphene or ITO electrode. (a) Current density and luminance versus voltage. Inset illustrates OLED layer stack comprising ITO or graphene bottom electrode and a MoO_3 hole-injection layer. (b) Current and power efficiency versus luminance. Inset shows photograph of powered graphene-based OLED at high brightness level.

To obtain lower sheet resistances we also doped few-layer graphene with MoO_3. With bi-layer graphene we obtained a sheet resistance of ~200 Ω/sq, with 3-layers of ~70 Ω/sq and with 4-layers of ~30 Ω/sq. The results imply that the MoO_3 induced charge transfer doping is effective over several graphene layers; however, the underlying mechanisms are not yet fully understood and will be discussed elsewhere. We measured the corresponding optical transmission with a 5 nm MoO_3 layer to vary between 94% and 86% at 550 nm for monolayer and 4-layer graphene, respectively. The MoO_3 doping of few-layer graphene is a promising concept to reach very low sheet resistance values without compromising the optical properties which can compete with state-of-the-art ITO electrodes grown on plastic foil paving the way for large area flexible OLED applications.

We evaluate the performance of our MoO_3-doped monolayer graphene by using it as an electrode in a bottom-emitting OLED device architecture, as schematically shown in Fig. 6a. We introduce a 150 nm thick MoO_3 doped CBP layer to further planarize the MoO_3 doped graphene surface. In previous literature, hole-injection layers with planarization properties such as PEDOT:PSS have been used, which however can deteriorate the device performance, because of its water content and acidic nature[32,33]. Also MoO_3 has been introduced in organic devices but either as wetting layer for PEDOT:PSS or as hole-injection layer[11,12,14]. We emphasize here that very efficient graphene-based OLEDs have been demonstrated by introducing a PEDOT:PSS or a work function modified PEDOT:PSS interlayer[13,15]. The doping was in both cases accomplished in a separate process, e.g. soaking the graphene samples in triethyloxonium hexachloroantimonate (OA)/dichloroethene solution or exposing to HNO_3 or $AuCl_3$. The combination of a metal-oxide induced optimum band alignment and stable doping of graphene that we use here allows for simplified, industry-compatible processing and neither requires any additional pre-treatment steps (involving partly aggressive and harmful chemicals, such as HNO_3 or $AuCl_3$), nor requires any additional solution process for a PEDOT:PSS interlayer. Fig. 6a and 6b show the measured OLED device characteristics. The efficient hole-injection from graphene and ITO electrodes via MoO_3 into the devices can be seen from the very low and almost identical onset-voltage of around 2.5 V. Photoemission spectroscopy studies have identified that also the charge transport from MoO_3 into CBP is nearly barrier-free[16]. Thus, the layer sequence graphene/MoO_3/CBP forms a highly suitable anode contact for efficient charge injection into OLEDs. The slope of the *JV*-curves indicates that the graphene monolayer-based OLED is somewhat electrically inferior due to the limited conductivity of the monolayer. However, this is compensated by a higher current efficiency of 55 cd/A at 1000 cd/m² leading to an overall superior power efficiency compared to the state-of-the-art ITO reference device. The lower light absorption and the lacking wave guide mode in the extremely thin graphene layer might reduce some optical loss channels and therefore enhance in particular the current efficiency compared to ITO.

We also evaluated OLEDs with a tri-layer graphene electrode, as shown in Fig. 7a and b. Compared to the ITO reference electrode, Fig. 7 highlights a very similar hole-injection for the tri-layer graphene based device as a result of the transport level matching. Please note that the device efficiencies should not be directly compared to Fig. 6 above, due to the slightly modified device stack architecture with a different emitter material. Despite the higher absorption of the tri-layer, graphene-based OLEDs with higher current and power efficiencies as with the ITO electrode are achieved. In addition, the low sheet resistance of the tri-layer graphene electrode (around 70 Ω/sq) leads to *JV*-characteristics which are very similar to the corresponding ITO devices. This indicates that the electrical limitations of the graphene monolayer can be overcome by using MoO_3 doped few-layer graphene.

In conclusion, we established a detailed understanding of metal oxide induced band alignment and charge transfer doping of graphene electrodes and demonstrate that such interface engineering in combination with a low sheet resistance is of key importance to achieve graphene-based OLED devices with superior efficiencies compared to state-of-the-art ITO electrodes. The extensive study of transition metal oxide based band engineering has played a key role in advancing the device structure and performance of ITO based organic electronics. Our study highlights that such band engineering is of even higher importance for graphene-based electrodes and their many future applications.

Methods

A low-pressure chemical vapor deposition process was used for the monolayer graphene synthesis on commercial, cold-rolled Cu foils (Alfa Aesar Puratronic, 99.999% purity, 25 μm thick) as described in detail elsewhere[5,22].

After synthesis, a poly (methyl methacrylate) (PMMA 495K diluted to 2% in Anisole) support layer was deposited on graphene on Cu and either 0.5 M aqueous solution of $FeCl_3$ or 0.1 M aqueous solution of $(NH_4)_2S_2O_8$ was used to etch the Cu foil. This was followed by multiple rinses in DI water after which MLG-PMMA stack was transferred to the desired substrate (SiO_2 (300 nm)/Si or glass substrates i.e. SiO_2 1.4 mm thick) and dried. The PMMA support layer was dissolved using hot acetone followed by a rinse in isopropanol and blow dried in nitrogen. Finally, the transferred samples were annealed in 4 mbar H_2 at ~300°C for 60 minutes to remove residual PMMA post transfer.

All organic and inorganic layers were prepared by thermal evaporation in a custom-built deposition system at a base pressure of 10^{-6} mbar. As substrates we used cleaned ITO pre-coated glass and graphene transferred on glass, respectively. The OLED stack comprises a 5 nm MoO_3 layer, a 150 nm MoO_3 doped 4,4′-Bis(*N*-carbazolyl)-1,1′-biphenyl (CBP) hole transport layer (20 wt%), a 10 nm CBP intrinsic transport layer, a double emission layer comprised of 7.5 nm CBP and

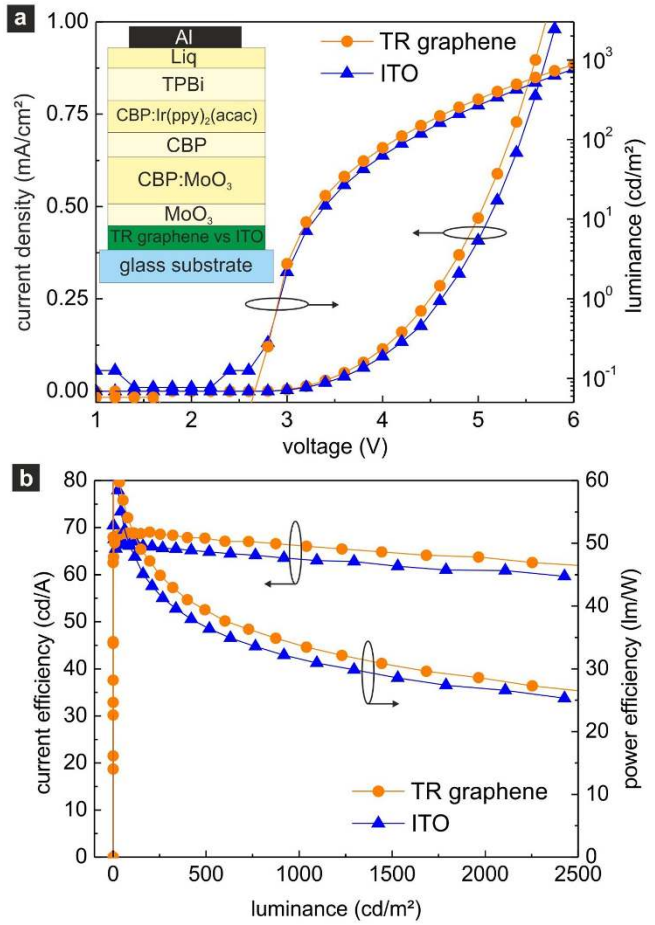

Figure 7 | Device characteristics of OLED stacks with either tri-layer (TR) graphene or ITO electrode. (a) Current density and luminance versus voltage. (b) Current and power efficiency versus luminance Inset shows photograph of powered graphene-based OLED at high brightness level.

7.5 nm 1,3,5-tris-phenyl-2-benzimidazolyl-benzene (TPBi) both doped with the green phosphorescent emitter materials fac-tris-2-phenylpyridine iridium ($Irppy_3$) with 10 wt%, a 45 nm TPBi electron transport layer, a 1 nm LiF electron injection layer and a 100 nm Al cathode. For the tri-layer OLED study, a 15 nm CBP doped with bis(2-phenylpyridine)(acetylacetonate)iridium(III) [$Ir(ppy)_2(acac)$] (10 wt%) was used as emission layer and 1 nm 8-hydroxy-quinolinato lithium (Liq) as electron injection layer. In-situ 4-point probe measurements were conducted in vacuum at a base pressure of 10^{-6} mbar. The graphene samples were heated up to 140°C in vacuum to remove contamination due to air exposure. Then MoO_3 was evaporated with a deposition rate of 0.1 Å/sec on the graphene samples and the change of sheet resistance was monitored.

XPS and UPS measurements were performed in a multi-chamber VG Microlab 300 A ESCA system with a base pressure of around 10^{-8} Pa. The analysis chamber was equipped with an X-ray source with a Mg/Al double anode for XPS and a differentially pumped, windowless discharge lamp for UPS. The UPS spectra were recorded using He–I radiation and for XPS Mg (Kα) radiation was used. The ionization energy IE was calculated from the energetic difference in the UPS spectrum between the onset of photoemission and the valence band edge of the metal oxide films. The work function WF was derived from the onset of photoemission in combination with the known position of the Fermi energy.

1. Gordon, R. G. Criteria for Choosing Transparent Conductor. *MRS Bull.* **25**, 52–57 (2000).
2. Butt, H. *et al.* Visible Diffraction from Graphene and Its Application in Holograms. *Adv. Opt. Mater.* **1**, 869–874 (2013).
3. Mak, K. F., Ju, L., Wang, F. & Heinz, T. F. Optical spectroscopy of graphene: from the far infrared to the ultraviolet. *Solid State Commun.* **152**, 1341–1349 (2012).
4. Nair, R. R. *et al.* Fine structure constant defines visual transparency of graphene. *Science* **320**, 1308–1308 (2008).
5. Kidambi, P. R. *et al.* Observing graphene grow: catalyst-graphene interactions during scalable graphene growth on polycrystalline copper. *Nano Lett.* **13**, 4769–4778 (2013).
6. Dean, C. R. *et al.* Boron nitride substrates for high quality graphene electronics. *Nature Nano.* **5**, 722–726 (2010).
7. Novoselov, K. S. *et al.* Two-dimensional atomic crystals. *PNAS* **102**, 10451–10453 (2005).
8. Wang, Y., Chen, X., Zhong, Y., Zhu, F. & Loh, K. P. Large area, continuous, few-layered graphene as anodes in organic photovoltaic device. *Appl. Phys. Lett.* **95**, 063302 (2009).
9. Sun, T. *et al.* Multilayered graphene used as anode of organic light emitting devices. *Appl. Phys. Lett.* **96**, 133301 (2010).
10. Wu, J. *et al.* Organic light-emitting diodes on solution-processed graphene transparent electrodes. *ACS Nano* **4**, 43–48 (2010).
11. Park, H., Brown, P. R., Bulovic, V. & Kong, J. Graphene as transparent conducting electrodes in organic photovoltaics: studies in graphene morphology, hole transporting layers, and counter electrodes. *Nano Lett.* **12**, 133–140 (2012).
12. Wang, Y., Tong, S. W., Xu, X. F., Özyilmaz, B. & Loh, K. P. Interface Engineering of Layer-by-Layer Stacked Graphene Anodes for High-Performance Organic Solar Cells. *Adv. Mater.* **23**, 1514–1518 (2011).
13. Han, T.-H. *et al.* Extremely efficient flexible organic light-emitting diodes with modified graphene anode. *Nat. Photonics* **6**, 105–110 (2012).
14. Hwang, J. *et al.* Multilayered graphene anode for blue phosphorescent organic light emitting diodes. *Appl. Phys. Lett.* **100**, 133304 (2012).
15. Li, N. *et al.* Efficient and bright organic light-emitting diodes on single-layer graphene electrodes. *Nat. Commun.* **4**, 2294–2301 (2013).
16. Meyer, J. *et al.* Transition Metal Oxides for Organic Electronics: Energetics, Device Physics and Applications. *Adv. Mater.* **24**, 5408–5427 (2012).
17. Chen, Z. Y. *et al.* Surface transfer hole doping of epitaxial graphene using MoO3 thin film. *Appl. Phys. Lett.* **96**, 213104 (2010).
18. Xie, L. *et al.* Electrical Measurement of Non-destructively p-type Doped Graphene using Molybdenum Trioxide. *Appl. Phys. Lett.* **99**, 012112 (2011).
19. Hellstrom, S. L. *et al.* Strong and Stable Doping of Carbon Nanotubes and Graphene by MoOx for Transparent Electrodes. *Nano Lett.* **12**, 3574–3580 (2012).
20. Wu, Q.-H. *et al.* Electronic structure of MoO3-x/graphene interface. *Carbon* **65**, 46–52 (2013).
21. Kröger, M. *et al.* P-type doping of organic wide band gap materials by transition metal oxides: A case-study on Molybdenum trioxide. *Org. Electron.* **10**, 932–938 (2009).
22. Kidambi, P. R. *et al.* The parameter space of graphene chemical vapor deposition on polycrystalline Cu. *J. Phys. Chem. C* **116**, 22492–22501 (2012).
23. Lee, G.-H. *et al.* High-Strength Chemical-Vapor–Deposited Graphene and Grain Boundaries. *Science* **340**, 1073–1076 (2013).
24. Kanai, K. *et al.* Electronic structure of anode interface with molybdenum oxide buffer layer. *Org. Electron.* **11**, 188–194 (2010).
25. Lee, H. *et al.* The origin of the hole injection improvements at indium tin oxide/molybdenum trioxide/N,N′-bis(1-naphthyl)-N,N′-diphenyl-1,1′-biphenyl- 4,4′-diamine interfaces. *Appl. Phys. Lett.* **93**, 043308 (2008).
26. Irfan, I., Zhang, M., Ding, H., Tang, C. W. & Gao, Y. Strong interface p-doping and band bending in C60 on MoOx. *Org. Electron.* **12**, 1588–1593 (2011).
27. Papadopoulos, T. A. *et al.* Nature of the Interfaces Between Stoichiometric and Under-Stoichiometric MoO3 and 4,4′-N,N′- dicarbazolebiphenyl: A Combined Theoretical and Experimental Study. *Adv. Funct. Mater.* **23**, 6091–6099 (2013).
28. Meyer, J., Shu, A., Kröger, M. & Kahn, A. Effect of contamination on the electronic structure and hole-injection properties of MoO3/organic semiconductor interfaces. *Appl. Phys. Lett.* **96**, 133308 (2010).
29. Irfan *et al.* Energy level evolution of air and oxygen exposed molybdenum trioxide films. *Appl. Phys. Lett.* **96**, 243307 (2010).
30. Bae, S. *et al.* Roll-to-roll production of 30-inch graphene films for transparent electrodes. *Nature Nano.* 5, 574–578 (2010).
31. Pirkle, A. *et al.* The effect of chemical residues on the physical and electrical properties of chemical vapor deposited graphene transferred to SiO2. *Appl. Phys. Lett.* **99**, 122108 (2011).
32. So, F. & Kondakov, D. Degradation mechanisms in small-molecule and polymer organic light-emitting diodes. *Adv. Mater.* **22**, 3762–3777 (2010).
33. de Jong, M. P., van IJzendoorn, L. J. & de Voigt, M. J. A. Stability of the interface between indium-tin-oxide and poly(3,4-ethylenedioxythiophene)/poly(styrenesulfonate) in polymer light-emitting diodes. *Appl. Phys. Lett.* **77**, 2255 (2007).

Acknowledgments

Funding is acknowledged from EU FP7 programme Grafol (Grant No. 285275). S.H. acknowledges funding from EPSRC (Grant No. EP/K016636/1 and EP/H047565/1). P.R.K. acknowledges funding from the Cambridge Commonwealth Trust.

Author contributions

J.M. and S.H. conceived of, and wrote the paper. J.M., C.W. and A.K. performed charge transfer doping, PES analysis and OLED device studies. P.R.K. and B.C.B. synthesized and transferred graphene material, and provided detailed graphene analysis. A.C., A.P. and A.Z. prepared some multilayer graphene samples. S.H. coordinated the project. J.R. provided insights into the band engineering. All authors discussed the results and reviewed the manuscript.

Additional information

Supplementary information accompanies this paper at http://www.nature.com/scientificreports

Competing financial interests: The authors declare no competing financial interests.

How to cite this article: Meyer, J. *et al.* Metal Oxide Induced Charge Transfer Doping and Band Alignment of Graphene Electrodes for Efficient Organic Light Emitting Diodes. *Sci. Rep.* **4**, 5380; DOI:10.1038/srep05380 (2014).